




RESEARCH ARTICLE

Environmental constraints on the origin of life based on membrane formation: the role of salinity

Taren Ginter^{1,2,3}, Alix Dujardin^{1,2}, Sanne Roumans^{1,2}, Lynn J. Rothschild⁴ and Maikel C. Rheinstädter^{1,2} 

¹Department of Physics and Astronomy, McMaster University, Hamilton, ON, Canada

²Origins Institute, McMaster University, Hamilton, ON, Canada

³School of Interdisciplinary Science, McMaster University, Hamilton, ON, Canada

⁴Space Science & Astrobiology Division, NASA Ames Research Center, Moffett Field, CA, USA

Corresponding author: Lynn J. Rothschild; Email: lynn.j.rothschild@nasa.gov; Maikel C. Rheinstädter; Email: rheinstadter@mcmaster.ca

Received: 2 March 2024; **Revised:** 6 August 2024; **Accepted:** 22 September 2024

Keywords: effect of salinity on fatty membrane formation, fatty acids, fatty acid membranes, membrane formation, prebiotic membranes

Abstract

The environmental conditions for the origin of life are still not well-constrained, but membrane-bound structures must have been key to the origin of life. Membranes composed of fatty acids are promising candidates due to their simplicity and plausible prevalence in prebiotic environments. To assess the stability of membranes composed of fatty acids with tail lengths ranging from 12 to 16 carbons at different temperatures and sodium chloride concentrations that may have existed on the early Earth, we conducted all-atom molecular dynamics (MD) simulations. In the absence of salt (freshwater), none of the fatty acids exhibited bilayer formation, whether below or above their chain melting temperature. However, elevating the salt concentration from 0.15 M (saline solution), 0.5 M (seawater), 1 M (seawater tide pools), 3 M (salty tide pools) and 5 M (Dead Sea) resulted in the formation of stable bilayers. The 16-carbon fatty acid required lower salt concentration, while shorter, 12-carbon chain necessitated higher salt levels. Increasing the salt concentration led to three main effects: (1) increased bilayer thickness, (2) reduced area per fatty acid and (3) elevated deuterium order parameter of the chains, resulting in more robust membranes. Our simulations indicated that the salt cations aggregated on the bilayer surfaces, effectively mitigating repulsive interactions among hydrophilic fatty acid head groups. These findings suggest that fatty acid bilayers are more likely present in ancient waters connected to saltwater reservoirs, or seawater tide pools with elevated salt concentrations.

Contents

Significance statement	2
Introduction	2
Results	4
Salinity is the main driver of bilayer formation	4
The presence of salt leads to more densely packed and better ordered bilayer membranes . . .	5
Discussion	7
Salt is the biggest driver of membrane stability	10
Longer chains and low temperature support formation	10
Salt increases fatty acid packing and tail ordering	10
The role of salt for membrane formation and stability	10

Conclusion	13
Materials and methods	13
Fatty acids	13
Molecular dynamics (MD) simulations	13
Data analysis	15

Significance statement

While the formation of membranes is fundamental to cellular organization, it is not an evolutionary process in the traditional sense but a result of the physicochemical properties of molecules and their interactions. Evolutionary processes subsequently shaped the diversity and complexity of life, including the structures and functions of cellular membranes. Due to the chemical complexity of modern phospholipids, fatty acids have been proposed as the fundamental building blocks of simple membranous vesicles and protocells because they can be abiotically synthesized through basic Earth chemistry. We show that simple fatty acid membranes do not form in the absence of salt and suggest seawater tide pools and hydrothermal springs as the most promising prebiotic environments for the formation of basic membranous structures.

Introduction

Primitive cells (so-called protocells) played a crucial role in the transition from the prebiotic chemical world to the biological world (Schrum *et al.*, 2010). This transition likely involved the encapsulation of genetic material (Deamer and Barchfeld, 1982) and other molecules present in the environment. Warm little ponds (WLPs) have been proposed as one of the earliest environments for the origin of life, as speculated by Charles Darwin regarding the emergence of proteins (Follmann and Brownson, 2009). WLPs undergo cycles of dehydration and rehydration, which promote the polymerization of RNA, making them a plausible environment for the emergence of life (Follmann and Brownson, 2009; Da Silva *et al.*, 2015). They are also an ideal environment for salt-induced peptide formation, which is a proposed prebiotic pathway for the formation of biologically relevant oligomers (Rode, 1999). It is hypothesized that multilamellar membrane structures could have formed within these WLPs through wet–dry cycles, with material encapsulated between the layers (Deamer and Barchfeld, 1982). Vesicular encapsulation of RNA, which can act as an enzymatic-like catalyst and carry information capable of replication, could provide all the necessary components for the emergence of early protocells (Deamer and Barchfeld, 1982; Szostak *et al.*, 2001).

The importance of membranous structures and protocells is described in the ‘Lipid world’ hypothesis proposed by Segre *et al.*, who suggested that spontaneous self-assembly of amphiphiles into supra-molecular structures is a crucial component of the origins of life due to improved reaction rates, selective properties and potential for simple homeostatic systems (Segrè *et al.*, 2001). While modern cell membranes are typically composed of phospholipids, they are not suitable candidates for components of the initial membrane boundary structures due to their complexity and the need for advanced biochemistry for fabrication. Simple amphiphilic molecules are more likely candidates for the initial cell membranes (Deamer and Dworkin, 2005).

Biological membranes are essential components of cells, separating the interior of cells from their external environment and compartmentalizing different cellular functions. The basic structure of membranes involves the organization of lipids, proteins and other molecules. This arrangement is driven by the hydrophobic and hydrophilic properties of these molecules. The formation of biological membranes is not typically considered an evolutionary process in the same sense as the evolution of species over generations. Instead, membrane formation is a fundamental aspect of cellular biology and is more closely related to the self-organization of molecules driven by physicochemical forces, such as surface tension (Hatta, 2011), entropy of aggregation (Budin *et al.*, 2012) and thermodynamic properties (Lombard, 2014).

While the evolution of life involves changes in species over time through natural selection, the basic principles governing membrane formation have likely been conserved across the evolutionary history of living organisms. The emergence of the first cells involved the spontaneous formation of lipid bilayers. Over time, the complexity of membranes and their associated functions evolved as organisms diversified.

Modern cell membranes typically contain hundreds of lipid species (van Meer *et al.*, 2008; Sampaio *et al.*, 2011; Klose *et al.*, 2013; Harayama and Riezman, 2018). The diverse structure, distribution and composition of lipids impact the physical properties of membranes. Biological effects include the ability to withstand extremes in temperature and pressure, although the full biological effect of these variations is unknown (Harayama and Riezman, 2018). Modern cell membranes are typically composed of phospholipids, which can spontaneously form lipid bilayers in an aqueous environment (Bangham *et al.*, 1965). Although it has been proven that these lipids can be synthesized abiotically, it is unlikely that all of the necessary components for phospholipid membranes, let alone complex modern cell membranes, would be abundant in a prebiotic environment (Hargreaves *et al.*, 1977; Monnard and Deamer, 2002; Pohorille and Deamer, 2009; Ruiz-Mirazo *et al.*, 2014).

Additionally, primitive membranes would not have the same complex biosynthetic machinery and structure as modern bilayer cell membranes, so the origin of protocell membranes is typically attributed to spontaneous assembly of amphiphilic molecules (Deamer and Barchfeld, 1982; Hanczyc *et al.*, 2003; Maurer and Nguyem, 2015). These molecules can assemble into micelles, monolayers and bilayers (as highlighted in Fig. 1), to create early cell-like vesicles (Deamer *et al.*, 2002).

Fatty acids, or monocarboxylic acids, have been proposed as an alternative constituent of the first protocell membranes (Gebicki and Hicks, 1973; Hargreaves and Deamer, 1978; Walde *et al.*, 1994; Schrum *et al.*, 2010). Fatty acids consist of carbon chains with a methyl group at one end of the chain and a carboxyl group at the other end (Rustan and Drevon, 2005). Fatty acids have a simpler chemical composition than phospholipids, and prebiotic chemistry could more easily permit synthesis of the necessary fatty acids and amphiphilic compounds required for membrane formation (Schrum *et al.*, 2010). This chemical simplicity could also evolve towards modern phospholipid membranes through phosphorylation and addition of a second acyl chain to form phosphatic acid, which is a simple phospholipid (Schrum *et al.*, 2010). Fatty acids also have desirable membrane transport permeability properties resulting from the lipid dynamics associated with vesicles (Mansy, 2010). The permeability

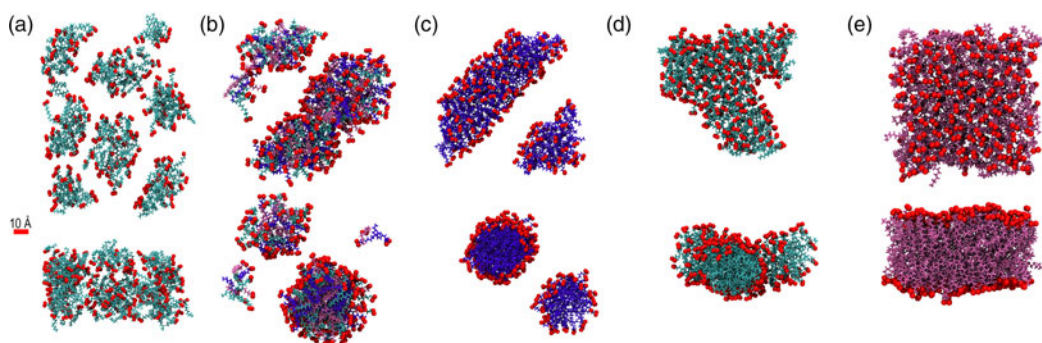


Figure 1. The fatty acids in this study were found to form distinct phases, depending on temperature and salinity. (a) Spherical micelles with average diameter ranging from 2 to 4 nm. (b) Larger spherical micelles began to group together with increasing salinity. (c) Example of cylindrical micelle formation which preceded bilayer formation. (d) Small bilayer patches began to form at elevated salt concentrations coexisting with cylindrical micelles. (e) Stable bilayer membranes with average thicknesses of approximately 1–1.5 nm formed for all fatty acids at the highest salt concentrations. Lauric acid (C12) is cyan, myristic acid (C14) is violet and palmitic acid (C16) is mauve. Water molecules and salt ions are not shown for clarity.

and the membrane growth associated with fatty acid membranes make them an ideal primitive membrane (Schrum *et al.*, 2010). They are permeable to small polar molecules and some charged molecules such as nucleotides, which suggests that cellular membranes could reasonably support the uptake of nutrients without modern transport mechanisms (Mansy *et al.*, 2008).

There is evidence that the necessary amphiphilic compounds were abundant in early Earth (Deamer *et al.*, 2002; Lazcano, 2010). Amphiphilic molecules isolated from the Murchison carbonaceous chondrite meteorite were found to be composed of varying acyl chain length and head group chemistry (Lawless and Yuen, 1979; Deamer, 1985; Deamer and Pashley, 1989). Other carbonaceous chondrites were also found to contain low-molecular weight fatty acids, suggesting that these simple amphiphiles may have been delivered to primitive Earth as a source of organics required to form simple membranes (Naraoka *et al.*, 1999). These findings matched simulated synthesis with UV photolysis of interstellar and precometary ice analogues (Dworkin *et al.*, 2001) and with Fischer–Tropsch reactions (McCullom *et al.*, 1999; Rushdi and Simoneit, 2001). This suggests that meteoritic delivery of fatty acids to the early Earth could support self-assembly of membranes (Deamer and Pashley, 1989).

While the exact chemical conditions at the origin of life remain uncertain, some key factors and conditions typically considered include the existence of energy sources such as ultraviolet (UV) radiation, lightning or geothermal heat; the availability of simple organic molecules; the presence of water, minerals and catalysts; different pH levels; and potentially reducing environments. In this study, we focus on the effect of salinity on the formation of prebiotic membranes made of simple fatty acid molecules. To describe the early environments that would have allowed the formation of fatty acid membranes, we conducted all-atom molecular dynamics (MD) computer simulations using 12, 14 and 16-carbon fatty acids (referred to as C12, C14 and C16), deprotonated fatty acids at various temperatures and salinity levels ranging from freshwater (no-salt conditions) to saline solutions, seawater, seawater tide pools, salty tide pools and up to Dead Sea salt levels. All simulations were performed at a neutral pH, but the use of deprotonated fatty acids mimics a basic environment. Our findings indicate that the presence of salt is the primary factor driving bilayer formation, with stable bilayers only forming at the highest salt concentrations for the short-chained fatty acid C12.

Results

MD simulations were performed using GROMACS and the CHARMM36 force field to investigate the behaviour of deprotonated C12, C14 and C16 fatty acids (lauric acid, myristic acid and palmitic acid). The simulations were conducted at temperatures both below and above the melting temperatures of the respective fatty acid. Detailed information about the simulation setup can be found in the ‘Materials and methods’ section. Six different salt conditions were simulated to mimic the range of potential salinities in aquatic bodies: no additional salt ions, 0.15 M NaCl, 0.5 M NaCl, 1 M NaCl, 3 M NaCl and 5 M NaCl. The 0.15 M NaCl concentration corresponds to physiologically relevant salt levels that resembles the conditions under which cells naturally operate, while 0.5 M is typical for present day seawater. Seawater tide pools can show elevated salt concentrations between 1 and 3 M due to evaporation. We also included a high salt concentration of 5 M NaCl comparable to the Dead Sea. Our investigation focused on studying the influence of fatty acid chain length, temperature and salinity on structure formation. The simulations started with an initial bilayer configuration, and if the bilayer was not stable, it typically dissolved within 30 ns, leading to the formation of spherical or cylindrical micelles, as shown in Fig. 1. Given the relatively fast structural dynamics observed, all simulations were run for a total simulation time of 50 ns.

Salinity is the main driver of bilayer formation

The complete phase diagram for all fatty acids at all temperatures and salt levels is shown in Fig. 2. Results are shown as a function of salt concentration for each fatty acid (C12, C14, C16) below and above the respective chain melting transition T_m . At 0 M NaCl, none of the fatty acids was found to

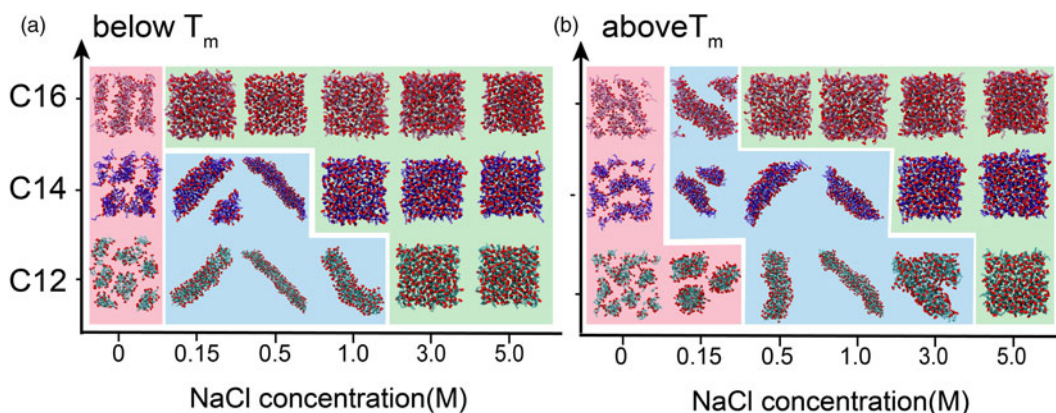


Figure 2. Phase diagrams for C12, C14 and C16. The fatty acids are represented along the vertical axis, and salinity increases along the horizontal axis. The red zones denote unstable phases, while blue indicates increased aggregation (such as cylindrical micelles), and green depicts stable bilayer membranes. (a) All simulations were performed below the respective fatty acid melting temperatures. C16 is the first fatty acid to form a stable membrane at 0.15 M NaCl. As salinity increases, the shorter-chain fatty acids begin to form stable membranes. (b) All simulations were performed above the fatty acid melting temperatures. Compared to (a), a higher salinity is required to promote fatty acid aggregation, and more simulations were observed in the intermediary phase. All simulations formed stable bilayer membranes at 5.0 M NaCl. Lauric acid (C12) is cyan, myristic acid (C14) is violet and palmitic acid (C16) is mauve. Water and salt molecules are not shown.

form stable membranes. All of the simulations yielded spherical micelles throughout the simulation boxes. When simulations were run below the chain melting temperature T_m , C12 and C14 were found to form cylindrical micelles at physiological salt concentrations of 0.15 M, while C16 was forming a stable bilayer in Fig. 2(a). Notably, higher salinity was required for the formation of membranes above T_m , which was highlighted by the salinity required for all fatty acids to form a stable membrane (3 M below T_m , and 5 M above T_m). Based on these observations, we propose that the phase sequence leading to more stable states progresses from spherical micelles to cylindrical micelles and eventually to bilayers. Transitions to more organized phases occurred when (1) the salt concentration was increased, and (2) longer-chain fatty acids were used. A higher salt concentration was needed at higher temperatures.

The presence of salt leads to more densely packed and better ordered bilayer membranes

To understand the effect of salt on the properties of the fatty acid bilayers, density profiles and thickness of stable membranes as a function of salt concentration were determined from the simulations, as described in ‘Materials and methods’ section. Figure 3(a) shows the density profiles of C16 bilayers as an example. The distinct peaks in density correspond to the position of the heavier oxygen atoms in the carboxylic acid head groups and were used to determine the position of the head group region.

As shown in Fig. 3(b) and (c), the thickness varied from approximately 0.28 to 1.35 nm. There was a significant increase in thickness with increasing salt concentration at temperatures below the chain melting temperature T_m , shown in Fig. 3(b). The thickness increase was less pronounced at temperatures above T_m in Fig. 3(c).

The deuterium order parameter, S_{CD} was used to examine the stability of the simulations based on the ordering of the lipid acyl chain tails. S_{CD} calculates the degree with which lipids are oriented and ordered based on the experimental procedure of measuring carbon–deuterium bond parameters with NMR spectroscopy. The order parameter is dependent on both the orientation of C–H bonds and

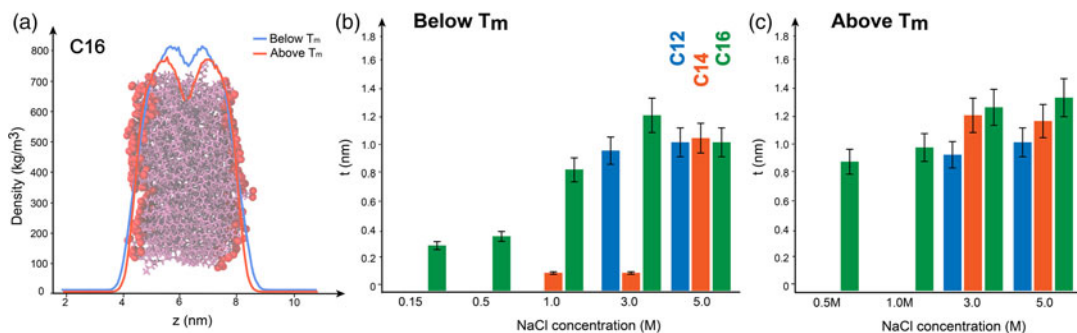


Figure 3. (a) Mass density profiles along the perpendicular z -direction of C16 bilayers at 5 M NaCl, where stable bilayers formed. The two maxima in the mass density correspond to the location of the heavier oxygen atoms in the fatty acid head groups, as shown in the overlaid snapshot of the simulation output for C16 below T_m at 5 M NaCl with water and salt not shown. (b) Bilayer thickness for the stable membrane-forming simulations for C12, C14 and C16 below T_m which increased with increasing salinity. (c) Thickness of all stable membranes for C12, C14 and C16 above T_m . Similarly to (b), there is a slight increase with increasing salinity. Numeric values for all parameters are given in Tables 1 and 2.

the disorder of the system. Low S_{CD} corresponds to disordered fatty acids in the membrane core. Longer chains can decrease S_{CD} due to increased alignment of the carbon bonds, and low temperatures typically correspond to higher S_{CD} due to lipids being packed together (Piggot *et al.*, 2017; Loschwitz *et al.*, 2020). S_{CD} was computed as described in ‘Materials and methods’ section. The S_{CD} profiles and average values for C16 simulations are shown in Fig. 4(a). C16 was the only fatty acid that formed a bilayer also at a lower salinity of 0.15 M NaCl and therefore allows a comparison between salt concentrations. Those S_{CD} profiles show values between 0.1 and 0.25, pointing at tightly packed and ordered fatty acids. S_{CD} profiles in micelles are significantly lower, with values of less than about 0.05. Average values for S_{CD} for all samples are plotted in Fig. 4(b) for C16 at temperatures below and above the chain melting transition. For both temperatures, increasing salinity led to an increase in the deuterium order parameter.

The area per fatty acid (area per lipid, APL) was determined for the simulations, and are listed in Tables 1 (for temperatures below T_m) and 2 (for above T_m). Values are also plotted in Fig. 5(a) and (b). The areas formed three distinct regimes: areas of about 0.85 nm² are typically found in loosely packed spherical micelles. More tightly packed areas of ~0.65 nm² indicate the formation of cylindrical micelles, while small areas around 0.4 nm² correspond to stable bilayers. The data points in Fig. 5(a) and (b) for temperatures below and above T_m follow the phase behaviour in the phase diagram in Fig. 2. The transitions from spherical micelles to cylindrical micelles and eventually to stable bilayers are accompanied with decreases in the areas per fatty acid, respectively.

We note that the areas in Tables 1 and 2 are in good agreement with Höltje *et al.* (2001), who report areas per fatty acid of ~0.35 nm² in fluid bilayers. We also note that areas of ~0.22 nm² were reported in this work and also earlier X-ray diffraction work in crystalline bilayers (Luzzati and Tardieu, 1974). Areas per fatty acid in simulations of mixed oleic acid/oleate bilayers also report areas of 0.30–0.35 nm², in good agreement with our values for fluid fatty acid bilayers (Han, 2013).

As membrane stability is typically correlated with lower APL values, these findings confirm the phase sequence in the phase diagram in Fig. 2, where the APL corroborates the increased stability with high salinity and low temperatures. These observations can be summarized as follows: increasing salt concentration leads to (1) an increase in bilayer thickness accompanied by (2) an increase in the deuterium order parameter S_{CD} , and (3) a decreased area per lipid. These findings are indicative of a more dense packing of the fatty acid tails in the presence of salt, with suppressed fluctuations.

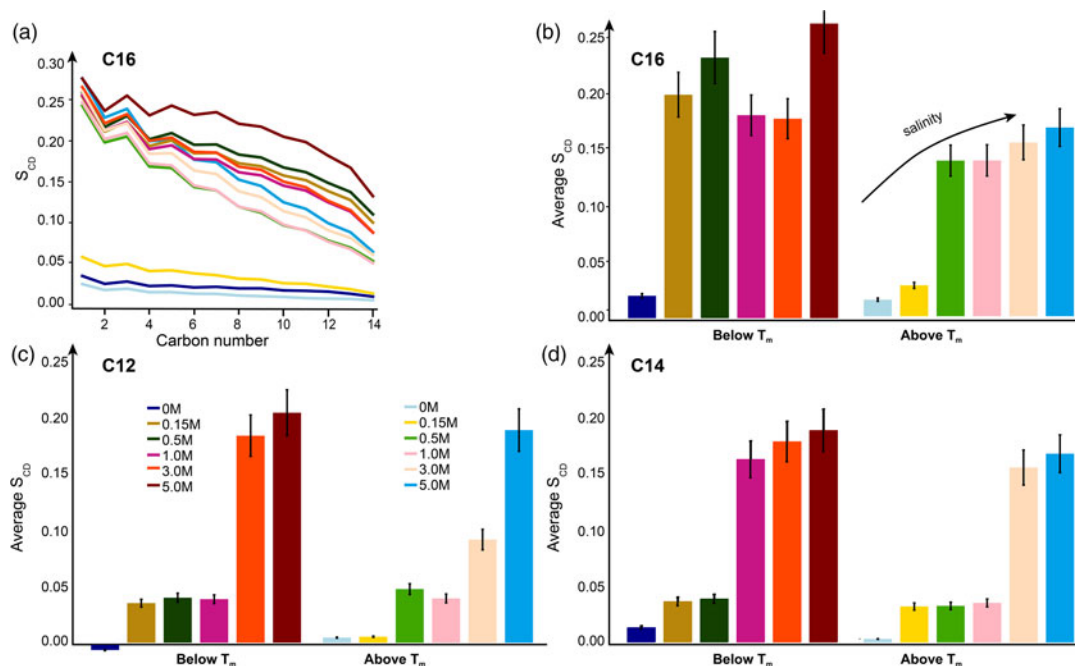


Figure 4. (a) Deuterium order parameter exemplary shown for C16 at different salt conditions and temperatures below and above the chain melting temperature. C16 formed a bilayer above salt concentrations of 0.15 M for low- T and above 0.5 M salt at high- T , as shown in the phase diagram in Fig. 2. Values for the order parameter in the bilayer phase were found to be significantly higher than values in the micelle phase. (b) Average values for the deuterium order parameter determined from the curves in part (a) for C16. For both temperatures, S_{CD} was found to significantly increase with increasing salt concentration. (c) Average deuterium order parameter of C12. (d) Average deuterium order parameter for C14. Error bars correspond to one standard deviation. Numeric values for all parameters are given in Tables 1 and 2.

Discussion

The formation of vesicular structures by oleic acid (C18) was first demonstrated through the mechanical agitation of evaporated long-chain fatty acids in buffer solution (Gebicki and Hicks, 1973, 1976). Subsequently, it was found that fatty acids can spontaneously self-assemble into vesicles in aqueous environments, similar to phospholipids (Gebicki and Hicks, 1973, 1976; Hargreaves and Deamer, 1978; Apel *et al.*, 2002; Monnard *et al.*, 2002). The stability of these vesicles was reported to be influenced by factors such as fatty acid chain length and composition, temperature, concentration and salinity (Apel *et al.*, 2002; Deamer *et al.*, 2002; Monnard *et al.*, 2002). Fatty acid bilayer membranes exhibit pH sensitivity due to the stabilization provided by van der Waals interactions and hydrogen bonding (Rosano *et al.*, 1969; Haines, 1983). The specific phases and structures formed through amphiphilic self-assembly depend on the packing behaviour of surfactants, which is governed by their soft matter characteristics and thermodynamic properties (Schäfer *et al.*, 2020).

Hargreaves and Deamer demonstrated that the presence of uncharged amphiphiles is necessary for the formation of membranes from ionic soaps and detergents. They observed the formation of liposomes from single-chain fatty acid amphiphiles and connected these liposomes to biomembranes through the visualization of permeability using phase-contrast microscopy (Hargreaves and Deamer, 1978). The fatty acid vesicles were found to be fluid and stable above the melting temperature. It was proposed that pH is linked to the pKa of lipid anions in the micelles, which affects their stability.

Table 1. Area per fatty acid (APL), average deuterium order parameter (S_{CD}) and membrane thickness for the last 20 ns of all simulations below T_m

Salinity (M)	Fatty acid	Area per lipid (nm ²)	Average S_{CD}	Thickness (nm)
0	C12	0.92 ± 0.012	-0.0023 ± 0.002	–
	C14	0.83 ± 0.004	0.014 ± 0.005	–
	C16	0.84 ± 0.003	0.020 ± 0.007	–
0.15	C12	0.70 ± 0.020	0.035 ± 0.010	–
	C14	0.64 ± 0.018	0.038 ± 0.011	–
	C16	0.42 ± 0.003	0.20 ± 0.036	0.28
0.5	C12	0.65 ± 0.021	0.040 ± 0.010	–
	C14	0.53 ± 0.013	0.041 ± 0.010	–
	C16	0.42 ± 0.004	0.23 ± 0.028	0.38
1.0	C12	0.68 ± 0.016	0.038 ± 0.011	–
	C14	0.40 ± 0.003	0.17 ± 0.051	0.097
	C16	0.40 ± 0.004	0.18 ± 0.044	0.80
3.0	C12	0.37 ± 0.001	0.18 ± 0.055	0.93
	C14	0.37 ± 0.002	0.19 ± 0.049	1.1
	C16	0.37 ± 0.002	0.18 ± 0.050	1.2
5.0	C12	0.34 ± 0.001	0.20 ± 0.051	1.0
	C14	0.35 ± 0.003	0.20 ± 0.050	1.0
	C16	0.34 ± 0.004	0.26 ± 0.025	0.98

Thickness values are only included for the stable membranes which had two distinct peaks corresponding to each bilayer. The high APL values are indicative of more loosely packed structures, such as spherical micelles, whereas the low APL values are related to closely packed fatty acids in stable membranes. S_{CD} and thickness correspond to the data shown in Figs 3 and 4.

Table 2. Area per fatty acid (APL), average deuterium order parameter (S_{CD}) and membrane thickness for the last 20 ns of all simulations above T_m

Salinity (M)	Fatty acid	Area per lipid (nm ²)	Average S_{CD}	Thickness (nm)
0	C12	0.93 ± 0.018	0.004 ± 0.002	–
	C14	0.79 ± 0.039	0.003 ± 0.001	–
	C16	0.86 ± 0.013	0.015 ± 0.006	–
0.15	C12	0.42 ± 0.083	0.005 ± 0.002	–
	C14	0.70 ± 0.015	0.034 ± 0.012	–
	C16	0.60 ± 0.010	0.028 ± 0.011	–
0.5	C12	0.97 ± 0.018	0.047 ± 0.013	–
	C14	0.59 ± 0.010	0.034 ± 0.012	–
	C16	0.43 ± 0.004	0.14 ± 0.058	0.92
1.0	C12	0.70 ± 0.009	0.039 ± 0.011	–
	C14	0.54 ± 0.008	0.037 ± 0.011	–
	C16	0.40 ± 0.002	0.14 ± 0.060	1.0
3.0	C12	0.48 ± 0.008	0.091 ± 0.020	0.90
	C14	0.38 ± 0.001	0.16 ± 0.059	1.2
	C16	0.38 ± 0.001	0.16 ± 0.059	1.3
5.0	C12	0.34 ± 0.0013	0.19 ± 0.059	1.1
	C14	0.36 ± 0.003	0.18 ± 0.061	1.2
	C16	0.35 ± 0.002	0.17 ± 0.063	1.4

Thickness values are only included for the stable membranes which had two distinct peaks corresponding to each bilayer. Similarly to the simulations below T_m , APL decreases with tightly ordered fatty acids in stable membranes. S_{CD} and thickness correspond to the data shown in Figs 3 and 4.

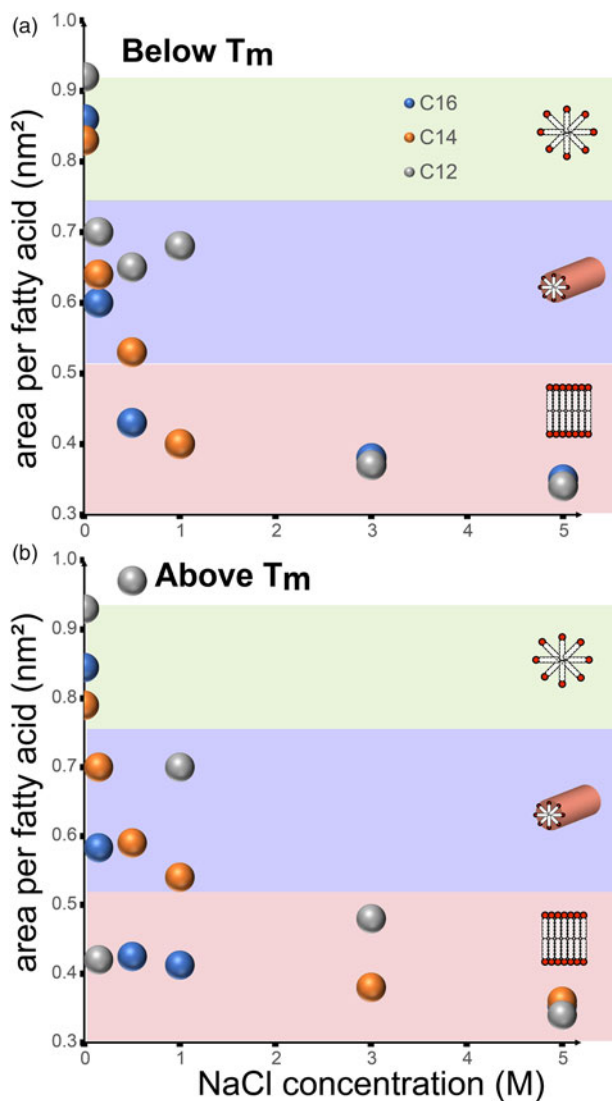


Figure 5. Area per fatty acid as a function of NaCl salt concentration. The areas fall into three distinct regimes: areas of about 0.85 nm^2 are found in loosely packed spherical micelles. More tightly packed areas of $\sim 0.65 \text{ nm}^2$ indicate the formation of cylindrical micelles, while small areas around 0.4 nm^2 correspond to stable bilayers. (a) Area for C16, C14, C12, below the respective chain melting temperature T_m . Formation of spherical micelles, cylindrical micelles and bilayers, with increasing salt concentration, in agreement with the phase diagram in Fig. 2. (b) Area per fatty acid above T_m .

For example, when saturated fatty acids were added to 1.0 M NaCl that is made acidic with 1.0 mM HCl (pH 3) and melted by increasing the temperature, the protonated fatty acids did not assemble into organized structures (micelles or bilayers) even though salt was present. Instead, they formed fluid droplets that floated on the surface. When the pH was then increased by titrating with NaOH to the pH that is also the pK of the carboxyl groups, the droplets dissolved into the aqueous phase as micelles, and subsequently formed vesicles if the fatty acid was sufficiently concentrated. In this case, the sodium ions brought along hydroxyl ions that adjusted the pH to the pK of the fatty acid, at which point half of the carboxyl groups became carboxylate anions (Maurer and Nguyen, 2015).

Salt is the biggest driver of membrane stability

Our findings suggest that at neutral pH, salt plays an important role in membrane formation and stability. For our simulations of deprotonated C12 (lauric acid), C14 (myristic acid) and C16 (palmitic acid), we did not observe stable bilayer membranes in pure water at pH 7, regardless of the fatty acids' chain length, or temperature. As the salinity increases, fatty acids aggregate into larger spherical micelles, cylindrical micelles and eventually stable bilayer membranes. These phases align with the existing literature on the self-assembly of amphiphiles, which is driven by the 'packing problem' (Schäfer *et al.*, 2020). Previous studies have shown that the binding of counter ions can lead to changes in micellar morphology, allowing stable cylindrical micelles to form (Schäfer *et al.*, 2020). The long-range interactions resulting from the presence of counter ions are responsible for the observed morphology transitions from spherical to cylindrical micelles before the fatty acid membranes stabilize. The packing of fatty acids in a manner similar to sodium dodecyl sulphate, as studied by Schäfer *et al.* (2020), further supports the role of forces in aggregation and determining the final shape. Additionally, Sangwai and Sureshkumar (2011) have shown that salt induces a phase transition from spheres to rods at high concentrations. The observed phase transitions from spherical to cylindrical micelles align with previous findings, reinforcing the significance of salt in shielding electrostatic interactions.

Once bilayers had formed, increasing salt concentration was found to lead to more densely packed and stable bilayers. Figure 6 illustrates MD snapshots of stable C16 membranes formed at 0.15 M NaCl and 5 M NaCl, which demonstrate the high salt affinity of the fatty acid bilayer surface. The positively charged Na^+ ions are attracted to and accumulate on the bilayer surface, particularly around the hydroxyl group and between the carboxylic acid head groups of the fatty acids.

The NaCl ions likely shield the electrostatic repulsion between fatty acid head groups, allowing for closer grouping of fatty acids. Ions can weakly bond to the charged head groups, creating an electric bilayer between the micelle–water surface, which results in a lower surface area per surfactant (Sangwai and Sureshkumar, 2011). The formation of a charged layer was also observed with the addition of antagonistic salts, which formed an electric double layer at the solvent interface and stabilized ordered structures such as membranes (Sadakane and Seto, 2018). The specific ions present play a role in how different salts impact charge shielding and the grouping of fatty acids (Hess and van der Vegt, 2009).

Longer chains and low temperature support formation

The only observed stable bilayer membrane at a moderate salt concentration of 0.15 M NaCl was formed by C16 fatty acids at a temperature below T_m , indicating that long chains and low temperatures support the formation of stable fatty acid membranes. This is further supported by the high S_{CD} values in this simulation, which indicate a higher degree of order in the fatty acid tails. However, the C16 0.15 M NaCl simulation above the melting temperature did not maintain a stable bilayer membrane; instead, it transitioned into a cylindrical micelle. The gel phase below T_m appears to promote membrane formation.

Salt increases fatty acid packing and tail ordering

Stable membranes formed at high salinity exhibited high deuterium order parameters, indicating a high degree of ordering in the fatty acids. In contrast, cylindrical and spherical micelle phases showed lower deuterium order parameters, corresponding to lower fatty acid ordering. The increased ordering of fatty acids supports the formation and retention of stable bilayer membranes, which is also reflected in the lower area per lipid and higher density of the stable membranes.

The role of salt for membrane formation and stability

While the presence of salt has been found to disrupt fatty acid membranes in some studies (for instance in Monnard *et al.*, 2002), our findings align with recent literature that supports the role of salts in shielding electrostatic repulsion and facilitating the formation of stable membranes. It is important

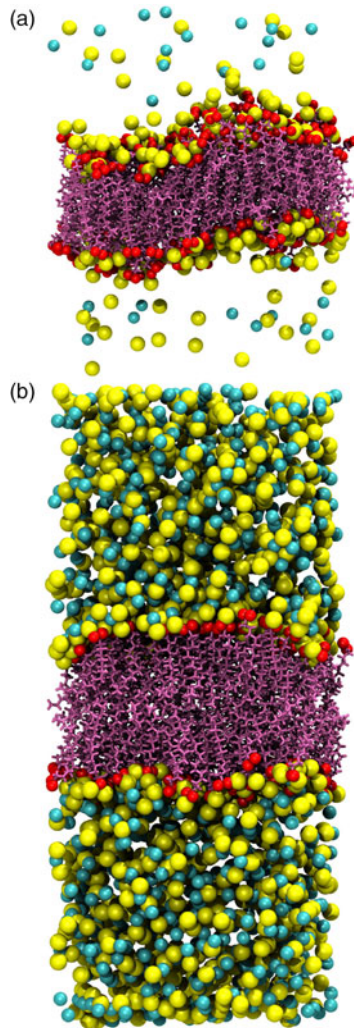


Figure 6. MD snapshots of (a) a stable C16 membrane below T_m at 0.15 M NaCl. The salt ions (yellow is sodium, teal is chloride) accumulate on the bilayer surface, between the fatty acid head groups. (b) Stable C16 membrane below T_m at 5.0 M NaCl. In both cases, the sodium ions were found to strongly interact with the bilayer surface, locating between the fatty acid head groups. Water molecules are not shown for clarity.

to note that the impact of salts on membrane formation can be complex and dependent on various factors. In our work, we specifically investigated the role of ion interactions resulting from environmental salt concentrations and their effect on the formation of stable fatty acid membranes.

Salt seems to be a significant factor in membrane stability. In highly saline environments, such as seawater tide pools or the Dead Sea, the presence of salt facilitates the formation of bilayer membranes from fatty acids. This suggests that a WLP located near a high salinity body of water, or a seawater tide pool, is a promising candidate for the emergence of protocells. Over time, salt concentrations in WLPs near less salty water sources, or tide pools, could increase through flooding by salty water and evaporation during wet–dry cycles. The salt ions play a crucial role in shielding the electrostatic repulsion between the hydrophilic heads of the fatty acids, allowing for closer contact and arranging themselves in a tightly packed and well-ordered membrane configuration, resulting in the formation of stable bilayer membranes. These findings are summarized in Fig. 7.

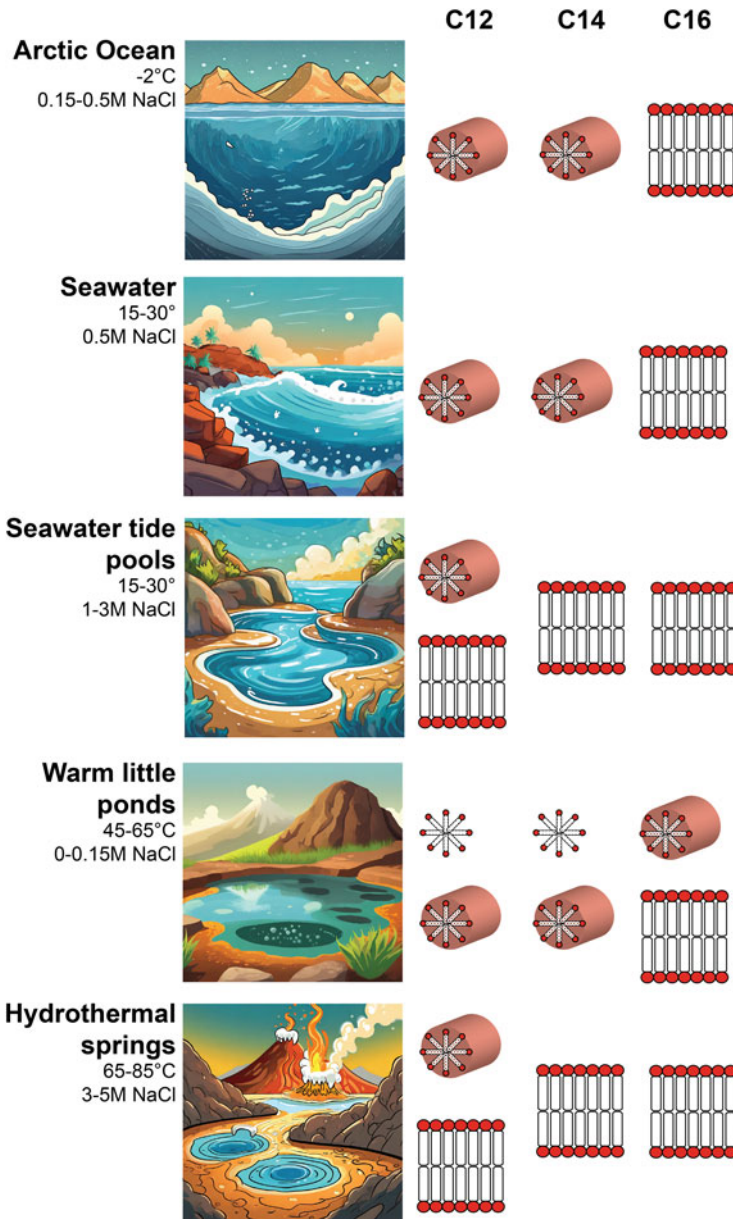


Figure 7. Summary of all results. Depending on temperature and salinity, fatty acids are expected to form micelles, cylindrical micelles or membranes. Seawater tide pools and hydrothermal springs should be most beneficial for the formation of membranous structures.

Although the high salinity values may appear to be unlikely in an early Earth environment, new estimates of halogen abundance in Earth's mantle suggest that seawater may have contained higher salt concentrations than modern Earth. The Halogen budget model presented by Guo and Korenaga proposes that halogens underwent early degassing and subsequent regassing, suggesting that halogen abundance may have been earlier than previously suggested for early Earth (Guo and Korenaga, 2021). Given that the current majority of halogens remain concentrated in surface reservoirs, including oceans (Kendrick *et al.*, 2017), an extremely salty body of water is a plausible environment for the emergence of prebiotic life.

Conclusion

The environmental conditions for the origin of life are not well constrained, but as membranes were key to the origin of life and the first ones were likely composed primarily of fatty acids, we conducted all-atom MD computer simulations to investigate the formation of bilayer membranes composed of C12, C14 and C16 fatty acids below and above their respective melting temperatures, and different salt concentrations to mimic freshwater ponds, saline solution, seawater, seawater tide pools, salty tide pools and dead sea salt concentrations. No bilayers formed in the absence of salt. The presence of NaCl facilitated fatty acid membrane formation by mitigating electrostatic repulsion, enabling the formation of tightly packed and highly ordered bilayer membranes. Longer fatty acid chains and lower temperatures also supported membrane formation. All fatty acids were found to undergo a phase sequence from spherical micelles to cylindrical micelles, and eventually bilayers. Phase coexistence was observed in the simulations. While the long-chained C16 can form bilayers already at physiological salt concentrations, C14 membranes would form in seawater tide pools only, and C12 bilayers require elevated salt concentrations of at least salty tide pools. Our findings suggest that fatty acids could likely serve as the fundamental building blocks for simple membranous vesicles and protocells in WLPs connected to salty water bodies, or seawater tide pools. Elevated salt levels in these ponds and pools can be maintained through the influx of salty water and the evaporation of water during wet–dry cycles. While the formation of membranes is a fundamental aspect of cellular organization, it is not an evolutionary process in the traditional sense but rather a result of the physicochemical properties of molecules and their interactions. Evolutionary processes would have subsequently shaped the diversity and complexity of life, including the structures and functions of cellular membranes.

Materials and methods

Fatty acids

All simulations were set up using the CHARMM-GUI (Jo *et al.*, 2008) bilayer builder (Wu *et al.*, 2014) using the built-in structures for lauric acid, myristic acid and palmitic acid. Table 3 lists these fatty acid properties.

Molecular dynamics (MD) simulations

Each fatty acid (C12, C14, C16) was simulated below and above the corresponding T_m with (1) no added ions, (2) 0.15 M NaCl, (3) 0.5 M NaCl, (4) 1.0 M NaCl, (4) 3.0 M NaCl and (5) 5.0 M NaCl. All systems contained 200 fatty acid molecules and 10 000 TIP3 water molecules (Mark and Nilsson, 2001). Salt molecules were added in accordance with the concentration and varied from no added sodium or chloride ions (0 M) to a maximum of 1176 sodium ion molecules and 976 chloride ion molecules, for a maximum system size of 12132 molecules in the systems containing 5.0 M NaCl. Transition temperatures are listed in Table 3. The plain membrane systems (systems which were only examining fatty acids on their own for the formation of bilayer membranes) all contained 100 deprotonated fatty acids on both the upper and lower leaflets. The membranes composed of equal parts C12, C14 and C16 deprotonated fatty acids contained 99 lipids on the upper and lower leaflets. The size of the simulation box was 419.4 nm³ (5.477 nm along the *x*- and *y*-axes, and 13.98 nm along the *z*-axis) for the plain membrane systems, and 415.0 nm³ (5.450 nm along the *x*- and *y*-axes, and 13.98 nm along the *z*-axis) for the mixed membranes. All systems contained 50 water molecules per one lipid molecule. The selected temperatures were about 15°C below and above T_m of each fatty acid. The bilayer builder in CHARMM-GUI was selected from the membrane builder input generator to set up the simulations. Each membrane was prepared with a rectangular box. The length of *z* was determined by the hydration number of 50 water molecules per 1 lipid molecule, and the length of *xy* was determined by the number of lipid components. The number and type of lipids used for each respective simulation were selected from the fatty acid drop-down menu to finalize the system information. NaCl ions were added in the

Table 3. List of all fatty acids used in this study, their chemical formula, the corresponding chain melting temperatures and the temperatures of the MD simulations

Fatty acid	Abbreviation	Formula	T_m (°C)	T_{sim} (°C)
Lauric acid	C12	$C_{12} H_{24} O_2$	44.35–46.35 (PubChem. Lauric Acid ; Human Metabolome Database)	27.85, 57.85
Myristic acid	C14	$C_{14} H_{28} O_2$	53.9 (PubChem. Hazardous Substances Data Bank (HSDB) ; PubChem. Myristic Acid)	38.85, 68.85
Palmitic acid	C16	$C_{16} H_{32} O_2$	61–63 (ICSC 0530 ; PubChem. Palmitic Acid)	47.85, 77.85

The simulation temperatures above and below the melting point were calculated as being 15°C below (referred to as ‘Below T_m ’) and 15°C above (‘Above T_m ’) to simulate a realistic environmental temperature fluctuation.

appropriate concentration using the replacement method for all systems that included ions. Once the ions and water box were generated, the CHARMM36m force field (Huang *et al.*, 2017) was chosen and the GROMACS input was selected. Finally, the temperature was adjusted to the corresponding simulation.

All-atom simulations were run using GROMACS 5.1.2 (Berendsen *et al.*, 1995; Lindahl *et al.*, 2001; Van Der Spoel *et al.*, 2005; Hess *et al.*, 2008; Pronk *et al.*, 2013; Abraham *et al.*, 2015; Páll *et al.*, 2015) on two GPU-accelerated computer workstations. The systems were first energy minimized using the steepest-descent algorithm. Minimization was followed by 250 ps of stepwise equilibration using an NVT ensemble with the reference temperature (corresponding to the specific simulation) maintained with the Berendsen thermostat. NVT equilibration was followed by 1625 ps of stepwise NPT equilibration at constant temperature (corresponding to the specific simulation) using the Berendsen thermostat. The pressure of 1.0 bar was maintained using the Berendsen barostat and semi isotropic weak coupling ($\tau = 5$ ps). Equilibration was confirmed with *gmx energy* to check for plateaus in the area per lipid and total energy. Following equilibration, simulations were performed for 50 ns using a 2 fs time step over 25 000 000 steps, a periodic boundary cut-off of 1.2 nm, the particle-mesh Ewald method using a real-space cut-off of 1.2 nm, fourth-order interpolation and 0.16 nm grid spacing to solve for long-range electrostatics. The parallel LINCS (P-LINCS) algorithm was used to determine bond constraints (Hess, 2008). Temperature and pressure were maintained at respective simulation temperatures (below T_m and above T_m) and 1.0 bar using a Nosé–Hoover thermostat (Nosé, 1984a, 1984b; Hoover, 1985) at 30°C ($\tau = 1.0$ ps) and Parrinello–Rahman semi isotropic weak coupling ($\tau = 5$ ps) (Parrinello and Rahman, 1981). All analyses were performed on the entire simulations and systems were run for 50 ns.

All MD simulations in this study were run at neutral pH 7 with respect to the CHARMM-GUI input generation. The challenge in explicitly defining pH directly in MD simulations arises from the fact that pH is a property that emerges from the behaviour of a large number of water molecules, ionizable solutes and their interactions (Hess and van der Vegt, 2009; Sadakane and Seto, 2018). At a pH of 7, a concentration of 10^{-7} M of H_3O^+ with water at 55 M means that effectively no water molecules are dissociated in a typical sized simulation box with less than 10^5 water molecules. We note that in fatty acid membranes, the protonation state of fatty acids can vary depending on the pH of the surrounding environment. Fatty acids contain a carboxylic acid group ($-COOH$), which can become protonated or deprotonated depending on the pH of the solution. At low pH (acidic conditions), the carboxylic acid group tends to be protonated, meaning it has picked up an extra hydrogen ion (H^+) to form the $-COOH$ group. In this protonated state, fatty acids have a net positive charge. At high pH (alkaline conditions), the carboxylic acid group tends to be deprotonated, meaning it has lost a hydrogen ion (H^+) to form the carboxylate anion ($-COO^-$). In this deprotonated state, fatty acids have a net negative charge.

C12–C16 fatty acids have pKa values in the range 4.95–5.3 ([Human Metabolome Database](#); [ICSC 0530](#); [PubChem. Hazardous Substances Data Bank \(HSDB\)](#); [PubChem. Lauric Acid](#); [PubChem.](#)

Myristic Acid; PubChem. **Palmitic Acid**). Using the Henderson–Hasselbalch equation, the ratio of protonated to deprotonated fatty acids was calculated for C12, C14 and C16 fatty acids with their respective pKa values. All three fatty acids are almost entirely deprotonated with pH above 7.0, so the acid is effectively dissociated. Using fully deprotonated fatty acids for all simulations essentially mimics a basic environment with pH >7. Our simulations are thus in agreement with reports that fatty acid membranes form in weakly alkaline conditions (pH 7–9) (Maurer and Nguyen, 2015).

Data analysis

GROMACS scripts were used to obtain the area per lipid, bilayer thickness and order parameter for the last 20 ns of each respective simulation. To calculate the area per lipid, *gmx energy* was used to extract the *x*- and *y*- box vectors from the portable energy file of the final output stage. The two vectors were then multiplied and subsequently divided by the number of lipids per leaflet (100 for the pure membranes analysed). The estimated error per *x*- and *y*- box vector was provided in the GROMACS output and propagated to the area per lipid.

gmx density was employed to compute the partial density of fatty acids across the simulation box. Only fatty acids were selected as the input to exclude the ions and water. The resulting *density.svg* files were uploaded to Python and the peak values of the high salt membranes were extracted using *find peaks* from *scipy.signal*. The change in thickness for stable membranes was calculated by taking the absolute difference of the *x* values (which correspond to the positions of fatty acids within the simulation box) associated with the density peaks of high salt membranes.

The order parameter was calculated using *gmx order*, which computes the order parameter for the atoms of carbon tails. An index file was first created which only contained the carbon atoms associated with the fatty acids. The index file was then used with *gmx order* to generate the order and the deuterium order parameter. Standard deviation was calculated from the average S_{CD} . The *deuter.svg* file was imported into Python to generate plots using matplotlib (Hunter, 2007), and simulation output images were created with visual molecular dynamics (Humphrey *et al.*, 1996).

Acknowledgements. We would like to thank Dr David Deamer, UC Santa Cruz, for fruitful discussions and advice on this project.

Financial support. This research was supported by the National Science and Engineering Council Canada (NSERC), the Canadian Foundation for Innovation (CFI) and McMaster University. M. C. R. is the recipient of an Early Researcher Award of the Province of Ontario and a McMaster University Scholar.

Competing interest. None.

References

- Abraham MJ, Murtola T, Schulz R, Páll S, Smith JC, Hess B and Lindahl E (2015) GROMACS: high performance molecular simulations through multi-level parallelism from laptops to supercomputers. *SoftwareX* **1–2**, 19–25.
- Apel CL, Deamer DW and Mautner MN (2002) Self-assembled vesicles of monocarboxylic acids and alcohols: conditions for stability and for the encapsulation of biopolymers. *Biochimica et Biophysica Acta (BBA) – Biomembranes* **1559**, 1–9.
- Bangham AD, Standish MM and Watkins JC (1965) Diffusion of univalent ions across the lamellae of swollen phospholipids. *Journal of Molecular Biology* **13**, 238–IN27.
- Berendsen HJC, van der Spoel D and van Drunen R (1995) GROMACS: a message-passing parallel molecular dynamics implementation. *Computer Physics Communications* **91**, 43–56.
- Budin I, Debnath A and Szostak JW (2012) Concentration-driven growth of model protocell membranes. *Journal of the American Chemical Society* **134**, 20812–20819.
- Da Silva L, Maurel M-C and Deamer D (2015) Salt-promoted synthesis of RNA-like molecules in simulated hydrothermal conditions. *Journal of Molecular Evolution* **80**, 86–97.
- Deamer DW (1985) Boundary structures are formed by organic components of the Murchison carbonaceous chondrite. *Nature* **317**, 792–794.
- Deamer DW and Barchfeld GL (1982) Encapsulation of macromolecules by lipid vesicles under simulated prebiotic conditions. *Journal of Molecular Evolution* **18**, 203–206.

- Deamer DW and Dworkin JP (2005) *Topics in Current Chemistry*. Berlin/Heidelberg: Springer-Verlag GmbH, pp. 1–27.
- Deamer DW and Pashley RM (1989) Amphiphilic components of the Murchison carbonaceous chondrite: surface properties and membrane formation. *Origins of Life and Evolution of the Biosphere* **19**, 21–38.
- Deamer D, Dworkin JP, Sandford SA, Bernstein MP and Allamandola LJ (2002) The first cell membranes. *Astrobiology* **2**, 371–381.
- Dworkin JP, Deamer DW, Sandford SA and Allamandola LJ (2001) Self-assembling amphiphilic molecules: synthesis in simulated interstellar/precometary ices. *Proceedings of the National Academy of Sciences of the USA* **98**, 815–819.
- Follmann H and Brownson C (2009) Darwin's warm little pond revisited: from molecules to the origin of life. *Naturwissenschaften* **96**, 1265–1292.
- Gebicki JM and Hicks M (1973) Ufasomes are stable particles surrounded by unsaturated fatty acid membranes. *Nature* **243**, 232–234.
- Gebicki JM and Hicks M (1976) Preparation and properties of vesicles enclosed by fatty acid membranes. *Chemistry and Physics of Lipids* **16**, 142–160.
- Guo M and Korenaga J (2021) A halogen budget of the bulk silicate Earth points to a history of early halogen degassing followed by net regassing. *Proceedings of the National Academy of Sciences* **118**, e2116083118.
- Haines TH (1983) Anionic lipid headgroups as a proton-conducting pathway along the surface of membranes: a hypothesis. *Proceedings of the National Academy of Sciences* **80**, 160–164.
- Han S (2013) Molecular dynamics simulation of oleic acid/oleate bilayers: an atomistic model for a ufasome membrane. *Chemistry and Physics of Lipids* **175–176**, 79–83.
- Hanczyc MM, Fujikawa SM and Szostak JW (2003) Experimental models of primitive cellular compartments: encapsulation, growth, and division. *Science* **302**, 618–622.
- Harayama T and Riezman H (2018) Understanding the diversity of membrane lipid composition. *Nature Reviews Molecular Cell Biology* **19**, 281–296.
- Hargreaves WR and Deamer DW (1978) Liposomes from ionic, single-chain amphiphiles. *Biochemistry* **17**, 3759–3768.
- Hargreaves WR, Mulvihill SJ and Deamer DW (1977) Synthesis of phospholipids and membranes in prebiotic conditions. *Nature* **266**, 78–80.
- Hatta E (2011) Surface tension driven instabilities in single-component saturated fatty acid membrane tubes. *Langmuir* **27**, 10400–10406.
- Hess B (2008) P-LINCS: a parallel linear constraint solver for molecular simulation. *Journal of Chemical Theory and Computation* **4**, 116–122.
- Hess B and van der Vegt NFA (2009) Cation specific binding with protein surface charges. *Proceedings of the National Academy of Sciences* **106**, 13296–13300.
- Hess B, Kutzner C, van der Spoel D and Lindahl E (2008) GROMACS 4: algorithms for highly efficient, load-balanced, and scalable molecular simulation. *Journal of Chemical Theory and Computation* **4**, 435–447.
- Höltje M, Förster T, Brandt B, Engels T, von Rybinski W and Höltje HD (2001) Molecular dynamics simulations of stratum corneum lipid models: fatty acids and cholesterol. *Biochimica et Biophysica Acta (BBA) – Biomembranes* **1511**, 156–167.
- Hoover WG (1985) Canonical dynamics: equilibrium phase-space distributions. *Physical Review A* **31**, 1695–1697.
- Huang J, Rauscher S, Nawrocki G, Ran T, Feig M, de Groot BL, Grubmüller H and MacKerell HD (2017) CHARMM36m: an improved force field for folded and intrinsically disordered proteins. *Nature Methods* **14**, 71–73.
- Human Metabolome Database: Showing metabocard for Dodecanoic acid (HMDB0000638). Available at <https://hmdb.ca/metabolites/HMDB0000638>
- Humphrey W, Dalke A and Schulten K (1996) VMD: visual molecular dynamics. *Journal of Molecular Graphics* **14**, 33–38, 27–28.
- Hunter JD (2007) Matplotlib: a 2D graphics environment. *Computing in Science & Engineering* **9**, 90–95.
- ICSC 0530 – Palmitic acid. Available at https://chemicalsafety.ilo.org/dyn/icsc/showcard.display?p_lang=en&p_card_id=0530&p_version=2
- Jo S, Kim T, Iyer VG and Im W (2008) CHARMM-GUI: a web-based graphical user interface for CHARMM. *Journal of Computational Chemistry* **29**, 1859–1865.
- Kendrick MA, Hémond C, Kamenetsky VS, Danyushevsky L, Devey CW, Rodemann T, Jackson MG and Perfit MR (2017) Seawater cycled throughout Earth's mantle in partially serpentinized lithosphere. *Nature Geoscience* **10**, 222–228.
- Klose C, Surma MA and Simons K (2013) Organellar lipidomics – background and perspectives. *Current Opinion in Cell Biology* **25**, 406–413.
- Lawless JG and Yuen GU (1979) Quantification of monocarboxylic acids in the Murchison carbonaceous meteorite. *Nature* **282**, 396–398.
- Lazcano A (2010) Historical development of origins research. *Cold Spring Harbor Perspectives in Biology* **2**, a002089.
- Lindahl E, Hess B and van der Spoel D (2001) GROMACS 3.0: a package for molecular simulation and trajectory analysis. *Molecular Modeling Annual* **7**, 306–317.
- Lombard J (2014) Once upon a time the cell membranes: 175 years of cell boundary research. *Biology Direct* **9**, 32.
- Loschwitz J, Olubiyi OO, Hub JS, Strodel B and Poojari CS (2020) Computer simulations of protein-membrane systems. *Progress in Molecular Biology and Translational Science* **170**, 273–403.

- Luzzati V and Tardieu A (1974) Lipid phases: structure and structural transitions. *Annual Review of Physical Chemistry* **25**, 79–94.
- Mansy SS (2010) Membrane transport in primitive cells. *Cold Spring Harbor Perspectives in Biology* **2**, a002188.
- Mansy SS, Schrum JP, Krishnamurthy M, Tobé S, Treco DA and Szostak JW (2008) Template-directed synthesis of a genetic polymer in a model protocell. *Nature* **454**, 122–125.
- Mark P and Nilsson L (2001) Structure and dynamics of the TIP3P, SPC, and SPC/E water models at 298K. *Journal of Physical Chemistry A* **105**, 9954–9960.
- Maurer SE and Nguyen G (2015) Prebiotic vesicle formation and the necessity of salts. *Origins of Life and Evolution of Biospheres* **46**, 215–222.
- McCollom TM, Ritter G and Simoneit BRT (1999) Lipid synthesis under hydrothermal conditions by Fischer–Tropsch-type reactions. *Origins of Life and Evolution of the Biosphere* **29**, 153–166.
- Monnard P-A and Deamer DW (2002) Membrane self-assembly processes: steps toward the first cellular life. *Anatomical Record* **268**, 196–207.
- Monnard P-A, Apel CL, Kanavarioti A and Deamer DW (2002) Influence of ionic inorganic solutes on self-assembly and polymerization processes related to early forms of life: implications for a prebiotic aqueous medium. *Astrobiology* **2**, 139–152.
- Naraoka H, Shimoyama A and Harada K (1999) Molecular distribution of monocarboxylic acids in Asuka carbonaceous chondrites from Antarctica. *Origins of Life and Evolution of the Biosphere* **29**, 187–201.
- Nosé S (1984a) A molecular dynamics method for simulations in the canonical ensemble. *Molecular Physics* **52**, 255–268.
- Nosé S (1984b) A unified formulation of the constant temperature molecular dynamics methods. *Journal of Chemical Physics* **81**, 511–519.
- Páll S, Abraham MJ, Kutzner C, Hess B and Lindahl E (2015) Tackling exascale software challenges in molecular dynamics simulations with GROMACS. In Markidis S and Laure E (eds), *Solving Software Challenges for Exascale*. Cham: Springer International Publishing, pp. 3–27. doi: 10.1007/978-3-319-15976-8_1.
- Parrinello M and Rahman A (1981) Polymorphic transitions in single crystals: a new molecular dynamics method. *Journal of Applied Physics* **52**, 7182–7190.
- Piggot TJ, Allison JR, Sessions RB and Essex JW (2017) On the calculation of acyl chain order parameters from lipid simulations. *Journal of Chemical Theory and Computation* **13**, 5683–5696.
- Pohorille A and Deamer D (2009) Self-assembly and function of primitive cell membranes. *Research in Microbiology* **160**, 449–456.
- Pronk S, Páll S, Schulz R, Larsson P, Bjelkmar P, Apostolov R, Shirts MR, Smith JC, Kasson PM, van der Spoel D, Hess B and Lindahl E (2013) GROMACS 4.5: a high-throughput and highly parallel open source molecular simulation toolkit. *Bioinformatics* **29**, 845–854.
- PubChem. Hazardous Substances Data Bank (HSDB): 5686. Available at <https://pubchem.ncbi.nlm.nih.gov/source/hsdb/5686>
- PubChem. Lauric Acid. Available at <https://pubchem.ncbi.nlm.nih.gov/compound/3893>
- PubChem. Myristic Acid. Available at <https://pubchem.ncbi.nlm.nih.gov/compound/11005>
- PubChem. Palmitic Acid. Available at <https://pubchem.ncbi.nlm.nih.gov/compound/985>
- Rode BM (1999) Peptides and the origin of life. *Peptides* **20**, 773–786.
- Rosano HL, Christodoulou AP and Feinstein ME (1969) Competition of cations at charged micelle and monolayer interfaces. *Journal of Colloid and Interface Science* **29**, 335–344.
- Ruiz-Mirazo K, Briones C and de la Escosura A (2014) Prebiotic systems chemistry: new perspectives for the origins of life. *Chemical Reviews* **114**, 285–366.
- Rushdi AI and Simoneit BRT (2001) Lipid formation by aqueous Fischer–Tropsch-type synthesis over a temperature range of 100 to 400°C. *Origins of Life and Evolution of the Biosphere* **31**, 103–118.
- Rustan AC and Drevon CA (2005) Fatty acids: structures and properties. In: *Encyclopedia of Life Sciences*. Chichester: John Wiley and Sons, Ltd., pp. 1–7. <https://doi.org/10.1038/npg.els.0003894>.
- Sadakane K and Seto H (2018) Membrane formation in liquids by adding an antagonistic salt. *Frontiers of Physics* **6**:26.
- Sampaio JL, Gerl MJ, Klose C, Ejsing CS, Beug H, Simos K and Shevchenko A (2011) Membrane lipidome of an epithelial cell line. *Proceedings of the National Academy of Sciences* **108**, 1903–1907.
- Sangwai AV and Sureshkumar R (2011) Coarse-grained molecular dynamics simulations of the sphere to rod transition in surfactant micelles. *Langmuir* **27**, 6628–6638.
- Schäfer K, Kolli HB, Christensen M, Bore SL, Diezemann G, Gauss J, Milano G, Lund R and Cascella M (2020) Supramolecular packing drives morphological transitions of charged surfactant micelles. *Angewandte Chemie International Edition* **59**, 18591–18598.
- Schrum JP, Zhu TF and Szostak JW (2010) The origins of cellular life. *Cold Spring Harbor Perspectives in Biology* **2**, a002212.
- Segrè D, Ben-Eli D, Deamer D and Lancet D (2001) The lipid world. *Origins of Life and Evolution of the Biosphere* **31**, 119–145.
- Szostak JW, Bartel DP and Luisi PL (2001) Synthesizing life. *Nature* **409**, 387–390.
- Van Der Spoel D, Lindahl E, Hess B, Groenhof G, Mark AE and Berendsen HJC (2005) GROMACS: fast, flexible, and free. *Journal of Computational Chemistry* **26**, 1701–1718.
- van Meer G, Voelker DR and Feigenson GW (2008) Membrane lipids: where they are and how they behave. *Nature Reviews Molecular Cell Biology* **9**, 112–124.

- Walde P, Wick R, Fresta M, Manngone A and Luisi PL (1994) Autopoietic self-reproduction of fatty acid vesicles. *Journal of the American Chemical Society* **116**, 11649–11654.
- Wu EL, Cheng X, Jo S, Rui H, Song KC, Dávila-Contreras EM, Qi Y, Lee J, Monje-Galvan V, Venable RM, Klauda JB and IM W (2014) CHARMM-GUI membrane builder toward realistic biological membrane simulations. *Journal of Computational Chemistry* **35**, 1997–2004.